

## Article

# Chitosan-Based Sustainable Coatings for Corrosion Inhibition of Aluminum in Seawater

Ana Alejandra Aguilar-Ruiz <sup>1</sup>, Germán Eduardo Dévora-Isiordia <sup>1</sup> , Reyna Guadalupe Sánchez-Duarte <sup>1,\*</sup> , Yedidia Villegas-Peralta <sup>1</sup>, Víctor Manuel Orozco-Carmona <sup>2</sup> and Jesús Álvarez-Sánchez <sup>1</sup> 

<sup>1</sup> Departamento de Ciencias del Agua y Medio Ambiente, Instituto Tecnológico de Sonora, 5 de Febrero 818 Sur, Ciudad Obregón C.P. 85000, Sonora, Mexico; ana.aguilar111695@potros.itson.edu.mx (A.A.A.-R.); gdevora@itson.edu.mx (G.E.D.-I.); yedidia.villegas@itson.edu.mx (Y.V.-P.); jesus.alvarez@itson.edu.mx (J.Á.-S.)

<sup>2</sup> Centro de Investigación en Materiales Avanzados S.C., Ave. Miguel de Cervantes 120, Complejo Industrial Chihuahua, Chihuahua C.P. 31136, Chih., Mexico; victor.orozco@cimav.edu.mx

\* Correspondence: reyna.sanchez@itson.edu.mx; Tel.: +52-644-4100900; Fax: +52-644-4109001

**Abstract:** Metals are widely used in various industrial applications due to their advantageous properties, but they often exhibit signs of degradation over time because of prolonged exposure to environmental conditions. To prevent corrosion, coatings have gained popularity owing to their practicality in maintaining the original shape and dimensions of the object being protected. Nevertheless, traditional coatings may pose significant toxicological and environmental concerns, leading researchers to explore eco-friendly alternatives such as chitosan-based coatings. Chitosan, a biopolymer derived from chitin, is abundant in nature and has been extensively studied for its physicochemical properties, including its potential in the development of new materials. Chitosan-based coatings have shown promise as effective corrosion inhibitors, and this study aims to develop a crosslinked chitosan-based coating from shrimp waste as an alternative to expensive, commercial coatings. Chitosan, and chemically modified polyethylene glycol, polyvinylpyrrolidone, and ammonium paratungstate chitosan coatings of high- and medium molecular weight prepared by the sol-gel technique, were used for the study of corrosion protection of aluminum in 3.5% synthetic seawater. The molecular interactions and structural alterations following cross-linking of chitosan-based coatings was supported by FTIR-ATR. Surface morphology analysis by AFM indicated good coating adsorption on aluminum surfaces. Contact angle measurements showed hydrophilic properties with contact angles  $>62^\circ$  and  $<90^\circ$ . Physicochemical characterization (molecular weight (kDa), deacetylation (%), humidity (%), and ash (%)) was also carried out. The corrosion inhibition effectiveness was assessed by gravimetric tests after immersion studies, and the results highlighted the MMW-Chi-based coating's performance.

**Keywords:** corrosion inhibition; aluminum; coatings; chitosan; cross-linking agents



**Citation:** Aguilar-Ruiz, A.A.; Dévora-Isiordia, G.E.; Sánchez-Duarte, R.G.; Villegas-Peralta, Y.; Orozco-Carmona, V.M.; Álvarez-Sánchez, J. Chitosan-Based Sustainable Coatings for Corrosion Inhibition of Aluminum in Seawater. *Coatings* **2023**, *13*, 1615. <https://doi.org/10.3390/coatings13091615>

Academic Editor: Yong X. Gan

Received: 23 August 2023

Revised: 7 September 2023

Accepted: 11 September 2023

Published: 15 September 2023



**Copyright:** © 2023 by the authors. Licensee MDPI, Basel, Switzerland. This article is an open access article distributed under the terms and conditions of the Creative Commons Attribution (CC BY) license (<https://creativecommons.org/licenses/by/4.0/>).

## 1. Introduction

Metals are frequently utilized in the construction of industrial structures, machinery, and equipment considering their advantageous properties, such as resistance to atmospheric factors, ductility, and thermal and electrical conductivity, among others. Nonetheless, prolonged use and exposure to environmental conditions often lead to signs of degradation or corrosion in the metal surface, and the species involved in this phenomenon may be toxic to human health and the environment [1]. Consequently, the degradation of these materials impacts the economy because of the replacement or restoration of the damaged units [2].

Corrosion can be defined as the deterioration of a material due to its exposure to certain environmental conditions, like acidic or alkaline media [3]. This problem can reduce the service life and hinder the optimal performance of equipment, necessitating their replacement in a relatively short time. It has been estimated that corrosion costs the global

industry USD 2.5 trillion, a figure equivalent to approximately 3.4% of world GDP [4]. Various techniques are available to prevent corrosion, principally coatings, galvanization, painting, and implementation of inhibitors like chromates and molybdates. Inhibitors are substances that interact with the metal surface or the surroundings, impeding corrosion through the reduction of diffusion, increasing anodic or cathodic polarizations, or just by reducing the diffusion of ions toward the material. The most employed techniques involve applying paints and varnishes. However, their anticorrosive pigments have been associated with substantial toxicological and environmental risks [5–7].

Coatings are increasingly being utilized because they function as a physical barrier between the substrate and the corrosive environment, thus preventing damage, while simultaneously serving as a storage place for inhibitor agents [8–10]. Coatings also offer the possibility of using natural polymers as a means of corrosion protection, thereby providing economic and environmental benefits. The main advantage of this approach is the low environmental impact and the potential to modify the polymer structure by incorporating corrosion inhibitors or cross-linking agents, unlike other anti-corrosion techniques [11,12]. Organic coatings based on biopolymers are commonly employed as an alternative to extending the lifespan of metals against corrosion, considering their eco-friendly nature that prevents the formation of harmful compounds. Nonetheless, these coatings encounter issues of adhesion and degradation in the presence of the metal and the surrounding environment, respectively. Consequently, a novel alternative approach is the use of organic coatings based on chitosan, a polysaccharide that can be attached to other compounds through ionic or cationic cross-linkages [13,14]. Chitosan is a biopolymer that can adsorb onto metal surfaces in its function as a corrosion inhibitor, forming a protective coating because of its inborn functional groups that serve as adsorption sites. Chitosan has an affinity for the metal surface, particularly the amino ( $-NH_2$ ) and hydroxyl ( $-OH$ ) groups. These electron-rich groups promote bond formation with the metal by interacting with it. It should be noted that the positively charged amino group ( $-NH_2$ ) contributes to this adsorption process, improving contact with the negatively charged metal surface [15].

Chitosan is primarily obtained from chitin, which is the second-largest natural polymer after cellulose. Chitin is widely distributed in the shells of crustaceans, crabs, insect shells, fungi, algae, mollusks, marine arthropods, and shrimp shells [16]. Chitin can be synthesized into chitosan through thermochemical deacetylation. Due to their amino cations, chitosan macromolecules have amazing qualities including hydrophilicity, non-toxicity, biodegradation, non-toxic, bacteriostatic, fungistatic, and excellent film-forming properties, high biocompatibility, and low cost. Food, healthcare, and other industries use chitosan extensively. Chitosan can also be modified through the addition of new elements enhancing its properties according to specific requirements. It has been noted in this regard that the mechanical, adhesive, and barrier characteristics of chitosan-based coatings can be successfully enhanced by incorporating organic and inorganic compounds; copolymerization is the most popular chitosan modification technique [17,18].

Chitosan has been therefore the subject of extensive research by numerous investigators due to its physicochemical properties. Its molecular structure permits various mechanical and chemical modifications, leading to intensified or acquired properties [19]. Furthermore, chitosan can interact with metal surfaces because of its active sites, which can form complexes with metal ions; as a result, chitosan is believed to have significant potential for developing new materials, primarily thanks to its biocompatibility property. The production of coatings based on modified chitosan has been considered a viable alternative, which could provide both mechanical and antimicrobial properties. This could help extend the metals' lifespan [20,21]. Several authors have investigated the anticorrosive properties of chitosan over the years utilizing its synergistic corrosion-inhibiting effect, specifically in hybrid, composite, or modified coatings, with results highlighting chitosan's defensive qualities significantly improved [22,23]. The benefits of crosslinked and raw chitosan offer a promising alternative to expensive and harmful coatings. Recent research has focused on the use of chitosan coatings for magnesium and steel alloys. However, there are not many

publications discussing the use of chitosan for aluminum and related alloys [24]. Finally, researchers encourage readers to think about the barrier corrosion protection provided by chitosan as a transient and reversible solution with a substantial research domain [25]. The goal of this research is to develop an alternative approach for corrosion inhibition of aluminum with medium- and high-molecular-weight crosslinked chitosan-based coatings; the crosslinking reagents used were ammonium paratungstate (PTA), polyethylene glycol (PEG), and polyvinylpyrrolidone (PVP). Shrimp shells, a waste product, will be used as the source of chitosan. The corrosion behavior was assessed by gravimetric tests, and the characterization of the substrate surfaces was performed by Fourier transform infrared spectroscopy (FTIR-ATR), contact angle, and atomic force microscopy (AFM) studies.

## 2. Materials and Methods

### 2.1. Reagents

Aluminum substrates cut into  $5 \times 5$  cm pieces were purchased from a local store. Chitosan was extracted from locally collected shrimp shells; 25% Glutaraldehyde (Glu), Ammonium paratungstate (PTA), and polyvinylpyrrolidone (PVP) were purchased from Sigma-Aldrich; 37.4% chlorohydric acid and Polyethylene glycol (PEG) were purchased from Merck; 99.5% acetic acid (glacial) and 99.5% acetone were purchased from FAGA lab; and synthetic seawater salt was obtained from Instant Ocean.

Chitosan characterization consisted of molecular weight determination by intrinsic viscosity measurements and molecular structure analysis through FTIR. Deacetylation degree, ash, and humidity percentage of chitosan were calculated. Coatings were characterized by contact angle, FTIR-ATR, and AFM studies. Finally, the coating's ability to inhibit the corrosion of aluminum in a corrosive medium was assessed by gravimetric tests.

### 2.2. Chitosan Extraction

Chitosan was synthesized by alkaline deacetylation of the chitin extracted from locally collected shrimps in a three-step process based on the methodology proposed by Sánchez-Duarte et al. [26], that involved demineralization, deproteinization, and deacetylation of chitin through hydrolysis of its acetamide groups with some modifications. Shrimp shells were washed and dried prior to the chemical treatment. First, the dried samples were demineralized in a 1 N HCl solution for 4 h at room temperature. Next, the demineralized samples were deproteinized with a NaOH 4.5% solution at 60 °C in an oil bath, stirring for 4 h. Finally, samples were deacetylated with NaOH 45% at 110 °C in an oil bath with stirring for 2 h for high-molecular-weight chitosan and 3 h for medium-molecular-weight chitosan. Chitosan flakes were washed thoroughly with distilled water until neutral pH was obtained, and then were allowed to dry at room temperature.

### 2.3. Aluminum Substrates Pretreatment

Aluminum substrates were sanded using sandpaper ranging from grade 200 to 2000, and then thoroughly rinsed with distilled water. Next, the sanded substrates were immersed in an acetone solution and subjected to ultrasonic treatment for 15 min to remove any residues from the sanded process and grease on the surfaces. The ultrasonicated substrates were subsequently rinsed with distilled water and air-dried at room temperature. Afterwards, the substrates were dipped into a 0.1 M NaOH dissolved in distilled water solution for 30 s, followed by a thorough distilled water rinse and drying in a drying oven Yamato DX402C for some time. The pretreated substrates were allowed to dry for 24 h at 60 °C in a drying oven. Finally, substrates were kept in a desiccator until ready for use.

### 2.4. Coatings Preparation

For the coating's preparation, the required solutions were elaborated prior to usage according to Table 1. Solution A was prepared by dissolving medium-molecular-weight chitosan (MMW-Chi) 1 *w/v*% in 2% acetic acid solution. For solution B preparation, the same procedure was followed using high-molecular-weight chitosan (HMW-Chi). Solution

C was prepared by adding glutaraldehyde to solution A in the relation 1:2, along with PEG in the relation 1:3. Solution D was prepared by adding glutaraldehyde and PEG in the relation 1:3 to the B solution. For solution E preparation, glutaraldehyde was added in the relation 1:2 to the A solution along with PEG maintaining the same relation. Solution F was prepared by adding glutaraldehyde and PVP in the relation 1:3 to the B solution. Solution G was prepared by dissolving PTA 1 mM in distilled water; 3.5% synthetic seawater was prepared by dissolving the seawater salt into distilled water.

**Table 1.** Coating preparation solutions.

Solution	Solute	Solvent	Coating
A	HMW-Chi	Acetic acid	HMW-Chi
B	MMW-Chi	Acetic acid	MMW-Chi
C	Glu + PEG	Solution A	HMW-Chi/PEG
D	Glu + PEG	Solution B	MMW-Chi/PEG
E	Glu + PVP	Solution A	HMW-Chi/PVP
F	Glu + PVP	Solution B	MMW-Chi/PVP
G	PTA	Distilled water	HMW-Chi/PTA MMW-Chi/PTA

Coatings were prepared according to the sol-gel technique and cured at room temperature. The procedure consisted of taking the pre-treated aluminum substrates into the precursor solutions of chitosan and its modifications (solutions A-F) and withdrawing them at the defined rate of 5 cm/min [27]. For the preparation of the Medium-Molecular-Weight Chitosan Coating (MMW-Chi), the pre-treated substrates were dipped into solution A, then withdrawn at the defined rate, and dried at room temperature for 24 h. For the High-Molecular-Weight Chitosan Coating (HMW-Chi), the same procedure was followed using solution B instead of solution A. Medium-Molecular-Weight Chitosan crosslinked with PEG coating (MMW-Chi/PEG) was prepared by dipping the pre-treated substrates into the C solution, withdrawing it, and drying at room temperature. The procedure was repeated for the High-Molecular-Weight Chitosan crosslinked with PEG coating (HMW-Chi/PEG) using solution D instead of solution C. The same procedure was repeated for the preparation of the Medium-Molecular-Weight Chitosan crosslinked with polyvinylpyrrolidone coating (MMW-Chi/PVP) and High-Molecular-Weight Chitosan crosslinked with polyvinylpyrrolidone coating (HMW-Chi/PVP) using solutions E and F, respectively.

For the preparation of High-Molecular-Weight Chitosan crosslinked with PTA and Medium-Molecular-Weight Chitosan crosslinked with PTA (HMW-Chi/PTA and MMW-Chi/PTA), the previously prepared MMW-Chi and HMW-Chi coatings were afterward crosslinked with PTA by impregnation, the coated substrates were immersed in solution G at a speed of 1 cm/min and kept in the solution for 15 min, and withdrawn immediately, rinsed with distilled water, and dried at room temperature for 24 h. Coated substrates were dried in the oven at 60 °C for at least 2 h and then kept on a desiccator until use. All coatings were prepared in triplicate.

### 2.5. Gravimetric Tests

To evaluate the corrosion inhibition ability behavior of the protective chitosan-based coated naked substrates, they were placed in flasks containing the 3.5% synthetic seawater solution previously prepared as a corrosive medium. The substrates were withdrawn and thoroughly rinsed with distilled water after 24, 48, and 72 h of immersion time at the beginning and then every week for up to 150 days. The rinsed substrates were dried in the oven at 60 °C for 12 h followed by weight measurement.

### 2.6. Chitosan Characterization Studies: MW and DDA

The molecular weight (MW) of the obtained chitosan was determined according to the technique described for Masuelli M [28] using the Mark–Houwink equation (Equation (1))

where  $\eta$  is the intrinsic viscosity,  $K$  and  $a$  are constants, and  $M_v$  is the average viscosimetric molecular weight to analyze the relation between the measured intrinsic viscosity and the viscosimetric molecular weight. An Ubbelohde capilar (Viscometer cal 100, Simga-Aldrich, St. Louis, MI, USA) was employed in a thermostatic bath ( $30 \pm 0.1$  °C). Humidity and ashes were measured following the previous method described by [26].

$$[\eta] = KM_v^a \quad (1)$$

The molecular structure and deacetylation grade (DDA) of the medium- and high molecular weight was determined using Fourier transform infrared spectroscopy (FTIR) on a Thermo Scientific Spectrum model Nico-let iS5, recorded under dry air at room temperature within the wave number range of  $400\text{--}4200$   $\text{cm}^{-1}$  with a spectral resolution of  $100$   $\text{cm}^{-1}$ .

### 2.7. Coatings Characterization Studies

Surface characterization of the coated substrates was carried out using Contact Angle, Molecular Structure, and Surface Morphology studies. The sessile drop method was assessed to determine the contact angle (CA) through Dataphysics equipment, model OCA 15EC, using the SCA20 1.0 software (Dataphysics, Filderstadt, Germany). The surface substrates analysis was measured on at least 5 spots; the results were presented as average along with the standard deviation. In order to analyze the coating's molecular structure Fourier transform infrared spectroscopy (FT-IR-ATR) studies were conducted. A small section from each coating was taken for analysis, which was subjected to freeze-drying to remove moisture. The freeze-dried samples were then analyzed using FTIR-ATR using a Fourier transform infrared spectrometer (Thermo Scientific Spectrum model Nicolet iS5, Waltham, MA, USA) recorded on KBr under dry air at room temperature within the wave number range of  $4000\text{--}500$   $\text{cm}^{-1}$  with a spectral resolution of  $100$   $\text{cm}^{-1}$ .

Surface morphology (SM) of the substrate surfaces was examined by atomic force microscopy (AFM workshop, Signal Hill, CA, USA) (model TT-AFM) before and after immersion in the corrosive medium. A solubility test was carried out by dissolving 2 g of chitosan in 10 mL of acetic acid and stirring for 24 h at 25 °C approximately.

## 3. Results and Discussion

### 3.1. Chitosan Characterization

The obtained molecular weight (MW), humidity, deacetylation degree, and ashes were determined as previously described and the results can be observed in Table 2. The MW of chitosan can vary in the range of  $80\text{--}1500$  kDa, and it is commonly classified into categories of low molecular weight (LMW), medium molecular weight (MMW), and high molecular weight (HMW) [27]. However, precise limits for each category of MW are not universally agreed upon, leading to some ambiguity in the literature.

**Table 2.** Medium- and High-Molecular-Weight Chitosan characterization.

	High Molecular Weight	Medium Molecular Weight	Reported	References
Molecular weight (kDa)	$463.49 \pm 0.99$	$397.43 \pm 0.99$	5–1500	[29,30]
Deacetylation (%)	$81.68 \pm 1.16$	$90 \pm 2.72$	50–95	[31,32]
Humidity (%)	$8.265 \pm 0.167$	$5.12 \pm 0.245$	7.6–13.10	[33,34]
Ash (%)	$0.497 \pm 0.03$	$0.2278 \pm 0.09$	0.2–5.50	[35]

Reported values are the average of  $n = 3$  standard deviation.

Some studies report that chitosan with a MW below 50 kDa is considered LMW chitosan, while chitosan with a MW ranging from  $50\text{--}150$  kDa falls within the MMW category. Nevertheless, other researchers consider chitosan with a MW greater than 50 kDa as HMW [36,37]. Regardless, different limits have been proposed by other authors for these categories. For example, some researchers suggest that LMW chitosan must be below

100 kDa, while the range of 100–1000 kDa is categorized as MMW chitosan, and HMW refers to chitosan greater than 1000 kDa [38,39].

It is worth mentioning that these classifications may vary among studies and depend on the criteria established by each author. The values for the MMW and HMW chitosan used in this study can be found in Table 2. The average MW of the chitosan obtained after 2 h in the deacetylation treatment was 463.493 kDa (HMW), and for the chitosan obtained after 3 h in the deacetylation treatment, the average was 397.43 kDa (MMW). The MW classification established in this work was consistent with the classification exhibited by Villegas-Peralta et al. [40], where the MWs reported for medium and high MW chitosan were 322.17 kDa and 501.59 kDa, respectively. Similar classifications were addressed for authors like Umoren et al., Mouaden et al., and Chauhan et al. [29,30,41].

### 3.2. FTIR Analysis

In pursuit of identifying the functional groups of the coatings, as well as confirming the incorporation of crosslinking agents into the polymeric matrix of chitosan, infrared spectroscopy analysis was performed. The molecular structure of the High- and Medium-Molecular-Weight chitosan (HMW-chi and MMW-chi) was also investigated through Fourier transform infrared spectroscopy (FT-IR) and the results are presented in Figure 1. Stretching vibrations of O-H and N-H were detected at bands the  $3200\text{ cm}^{-1}$  and  $3500\text{ cm}^{-1}$ . The same vibrations were reported in studies published by Shamsheera et al. and Oliveira et al. [32,42]. The IR peaks at  $3455.03\text{ cm}^{-1}$  correspond to the O-H functional group of chitosan. The presence of carbon peaks (C-N, C-O-C bonds) at the bands  $1645\text{ cm}^{-1}$  and  $1570\text{ cm}^{-1}$  confirms the presence of amine, acetamide, and hydroxyl groups in chitosan [43]. The peak detected at  $2880\text{ cm}^{-1}$  corresponds to the stretching vibration of C-H bonds; the same behavior was reported by Sambyal et al. [9]. The bands at  $1420\text{ cm}^{-1}$  and  $1315\text{ cm}^{-1}$  were attributed to the flexion vibrations of O-H and C-H to N-H, respectively [32].

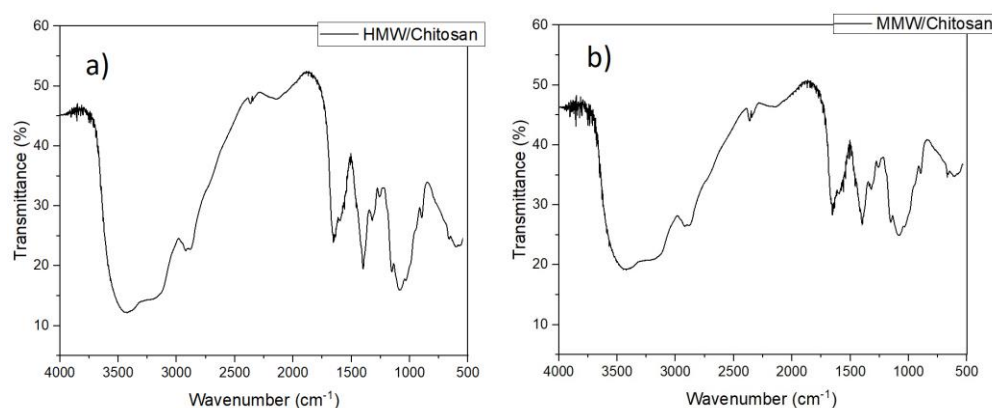


**Figure 1.** FTIR spectra for High-Molecular-Weight Chitosan (a) and Medium-Molecular-Weight Chitosan (b).

The molecular interactions of the individual HMW-chi and MMW-chi and their structural modifications after cross-linking were also investigated through FTIR; the results are presented in Figures 2 and 3. HMW-Chi spectra show the presence of O-H and N-H characteristic bonds of chitosan at the  $3200\text{ cm}^{-1}$  and  $3500\text{ cm}^{-1}$  peaks. The same behavior was reported by Sambyal et al. [9]. Characteristic stretching and flexion vibration bands of amide I and amine groups (C=O, N-H, O-H) were detected at the  $1660\text{ cm}^{-1}$  and  $1570\text{ cm}^{-1}$  peaks, along with the deformation vibration bands of the amide III group (C-H, N-H) at the  $1314\text{ cm}^{-1}$  peak. Bands at  $1150\text{ cm}^{-1}$  and  $894\text{ cm}^{-1}$  correspond to the presence of glycosidic bonds of chitosan [21–32]. Regarding the difference in the MW of the two chitosan coatings, no significant difference was observed. A weak signal of the C-H stretching vibration peak at  $2885\text{ cm}^{-1}$  C-H was detected for the HMW-chi/PVP and MMW-chi/PVP coating spectra presented in Figures 2 and 3 [44]. The  $1550$  y  $1650\text{ cm}^{-1}$  peaks corresponding to C=O and

CH<sub>2</sub> bending in pure chitosan are also shown, but at a lower intensity compared to the HMW and MMW chitosan spectra; this can be attributed to the increase in bond vibration intensity given for the presence of glutaraldehyde, and hence cross-linkage is demonstrated. The absorption bands observed approximately at 1250 and 1000 cm<sup>-1</sup> correspond to C-N and C-O stretching vibrations of the PVP structure, confirming the presence of PVP in the coating matrix for both HMW and MMW chi/PVP [45]. Pyrrolidone exhibited stretching absorption vibrations at 2947 cm<sup>-1</sup> of CH<sub>2</sub> and C=O groups, confirming the absorption of PVP in the matrix [46,47]. As can be observed in Figure 3, despite the difference in the MW for the HMW-chi/PEG and MMW-chi/PEG coatings, the spectra exhibited very similar behavior where peaks at approximately 2850 and 1250 cm<sup>-1</sup> were attributed to PEG presence. PEG addition shifted the C-O bands of the pure chitosan from 1660 to 1700 cm<sup>-1</sup> due to the stretching vibration of the PEG molecules [48]. Figure 2 demonstrates that the HMW-Chi/PTA spectra show characteristic peaks of PTA at 980 and 890 cm<sup>-1</sup>, which, according to Kalpakli et al. and Pecoraro et al. [49,50], corresponds to the P-O, W-O, and W-O-W bonds. The absorption peak at 2910 cm<sup>-1</sup> is attributed to the C-H stretching vibration and the 1570 cm<sup>-1</sup> peak of N-H bond reappeared at 1590 cm<sup>-1</sup> for both HMW and MMW-Chi/PTA spectra; similar results were obtained by [51].

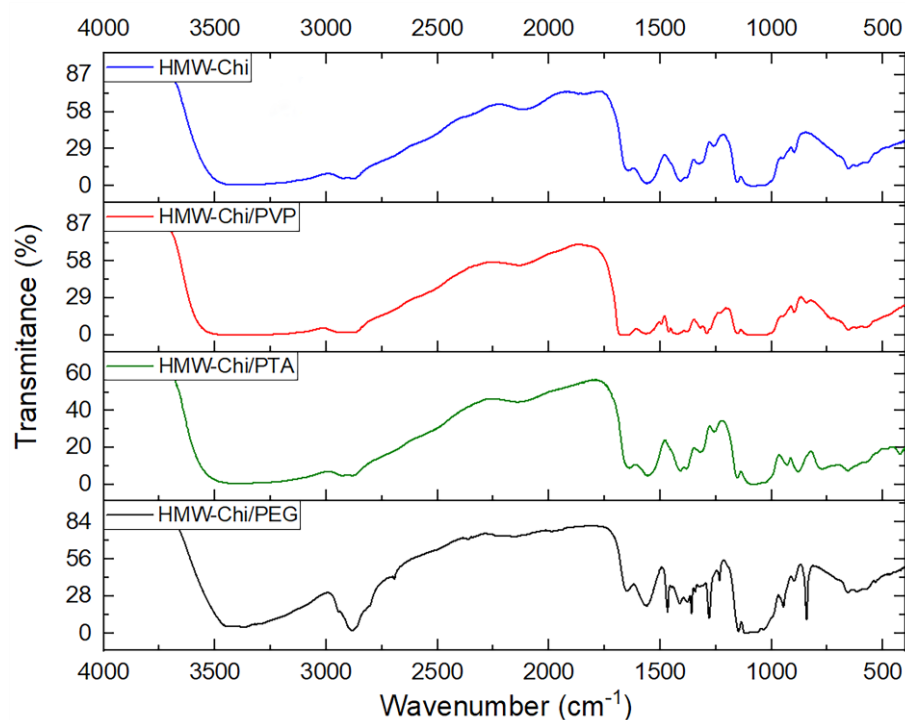


**Figure 2.** FTIR-ATR high-molecular-weight chitosan-based spectra.

### 3.3. Contact Angle

Contact angle analysis was used to determine the surface wettability of the chitosan and the chitosan-based coatings. In general terms, a surface is considered hydrophobic when it presents a contact angle of 90° or higher, and hydrophilic when it reports a contact angle below this [52]. Table 3 provides the average contact angle of all the samples. Contact angles for HMW-Chi and MMW-Chi were  $69.80 \pm 3.16^\circ$  and  $72.22 \pm 1.04^\circ$ , respectively; these results coincide with the results reported by authors like [24], who reported a contact angle for chitosan coatings of around 69°, and [53], who reported a contact angle of 71° for the chitosan. This hydrophilic characteristic is associated with the acetyl and amino groups present in the macromolecule of chitosan [54].

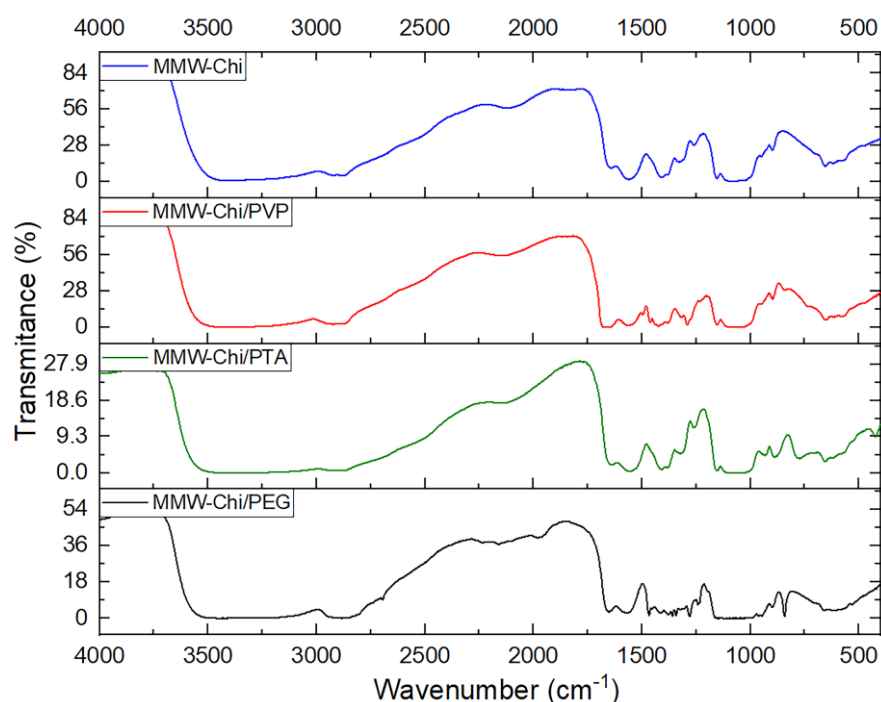


**Figure 3.** FTIR-ATR medium-molecular-weight chitosan-based spectra.

**Table 3.** Contact angle of medium- and high-molecular-weight chitosan coatings.

Coating Sample	Contact Angle (°)
HMW-Chi	69.80 ± 3.16
HMW-Chi/PTA	62.97 ± 3.43
HMW-Chi/PEG	73.00 ± 2.04
HMW-Chi/PVP	72.83 ± 3.08
MMW-Chi	72.22 ± 1.04
MMW-Chi/PTA	63.80 ± 3.08
MMW-Chi/PEG	67.92 ± 4.84
MMW-Chi/PVP	70.92 ± 5.08

Reported values are the average of  $n = 5$  standard deviation.

HMW-Chi/PTA contact angle slightly decreased in comparison to HMW-Chi contact angle, thus exhibiting a hydrophilic interaction between chitosan polymer chains and PTA. The same behavior was reported in the research of [12], where the native chitosan coatings changed from  $100^\circ$  to  $20^\circ$  after incorporating PTA. These results were accredited to the increased polarity of the surface due to the presence of ionic PTA in chitosan. Similar behavior was reported for the MMW-Chi/PTA coatings, where the contact angle was around  $63.80 \pm 3.08^\circ$ .

For HMW-Chi/PEG, the contact angle was expected to be lower due to the hydrophilic behavior of the PEG; nevertheless, the contact angle was approximately  $73 \pm 2.04^\circ$ . This could be attributed to the presence of glutaraldehyde in the matrix, which has a hydrophobic behavior, contrary to the PEG behavior. The given contact angle results were very similar to the  $77 \pm 1.46^\circ$  reported by [55]. MMW-Chi/PEG contact angle slightly decreased to  $67.92 \pm 4.84^\circ$  in comparison to MMW-Chi. The above can be ascribed to the strong hydrophilic behavior of the PEG and to the uncovered PEG area [43]. In this case, the result was slightly higher than the ones obtained and reported by authors like Bakmaz et al. [56], who reported contact angles that decreased as the PEG concentration increased from  $63.14^\circ$  to  $50.15^\circ$ .

HMW-Chi-PVP and MMW-Chi/PVP contact angles were  $72.83 \pm 3.08^\circ$  and  $70.92 \pm 5.08^\circ$ , respectively. These results are similar to those reported by [16]. In this work, the contact

angle reported for Chi-PVP was around  $79.3^\circ$  and as in the PEG case, with the increase in PVP concentration, the contact angle decreased, thus due to the hydrophilicity amino and carboxyl groups of PVP. In the present work, the contact angles reported for PVP coatings did not present a drastic drop, which could be attributed to the presence of glutaraldehyde in the coating's matrix.

In general terms, it was observed that HMW-Chi/PTA and MMW-Chi/PTA coatings exhibit lower contact angles compared to the other evaluated coatings. This suggests better wettability and higher affinity towards synthetic seawater. On the other hand, HMW-Chi/PEG, HMW-Chi/PVP, MMW-Chi/PEG, and MMW-Chi/PVP coatings showed slightly higher contact angles, indicating lower wettability compared to HMW-Chi/PTA and MMW-Chi/PTA coatings.

### 3.4. AFM Analysis

The surface morphology of the coatings, as well as the adsorption mode of the coating's protection at the subatomic level, were supported by AFM analyses. Table 4 presents the results in terms of roughness average (Ra) for naked and coated substrates. The substrates utilized for the essays were previously exposed to a chemical etching process with NaOH in the pre-treatment before the coating process, thus enhancing the increase in roughness parameters which allowed the coating to adhere more effectively to the substrate. Hu et al. and Zhang et al. [57,58] mentioned in their works that increased roughness before the coating process was observed to play an important role in determining the adhesion strength between the metal surface and the coating improving the bonding area.

**Table 4.** Average surface roughness parameter of naked aluminum and medium- and high-molecular-weight chitosan coatings.

Sample	Ra (nm)
Aluminum	$187.75 \pm 25.68$
HMW-chi	$24.95 \pm 3.74$
HMW-chi/PTA	$42.65 \pm 21.50$
HMW-chi/PEG	$47.94 \pm 10.49$
HMW-chi/PVP	$62.92 \pm 26.21$
MMW-chi	$90.52 \pm 10.98$
MMW-chi/PTA	$61.37 \pm 21.60$
MMW-chi/PEG	$52.95 \pm 37.02$
MMW-chi/PVP	$151.27 \pm 33.59$

Reported values are the average of  $n = 6$  standard deviation.

Ra for coated substrates exhibited a noticeable decrease in comparison to the Ra of the naked aluminum, thus enhancing the smoothness of the samples, which, according to Ashassi-Sorkhabi and Kazempour, and Srivastava et al. [22,59], could be attributed to the good adsorption of the coatings on the aluminum surface, thus conferring protection against corrosion, while the barely noticeable decrease in Ra for some may be attributed to a fine crack network formed when applying the coating blend over the samples [2]. In general terms, the notable decrease in the roughness parameter in the presence of the coatings could be beneficial for hindrance of the mass passage to avoid corrosion according to [42].

The AFM average surface roughness findings for the samples before and after 150 days of immersion in 3.5% synthetic seawater medium are presented in Table 5. It can be observed in the results that the unprotected aluminum Ra increases from 187.75 nm (Figure 4) to 417.25 nm after immersion time (Figure 5a). The increase in the surface roughness for the naked aluminum was directly related to the wear of the material.

**Table 5.** Surface roughness parameters of naked aluminum and medium- and high-molecular-weight chitosan coatings after 150 days of immersion in 3.5% synthetic seawater.

Sample	Ra after Immersion (nm)
Aluminum	417.25 ± 221.81
HMW-chi	147.175 ± 46.00
HMW-chi/PTA	202.02 ± 101.77
HMW-chi/PEG	322.05 ± 113.43
HMW-chi/PVP	113.00 ± 10.31
MMW-chi	223.21 ± 111.02
MMW-chi/PTA	232.21 ± 109.16
MMW-chi/PEG	154.75 ± 44.19
MMW-chi/PVP	269.81 ± 56.68

Ra is the roughness average surface. Reported values are the average of n = 6 standard deviation.

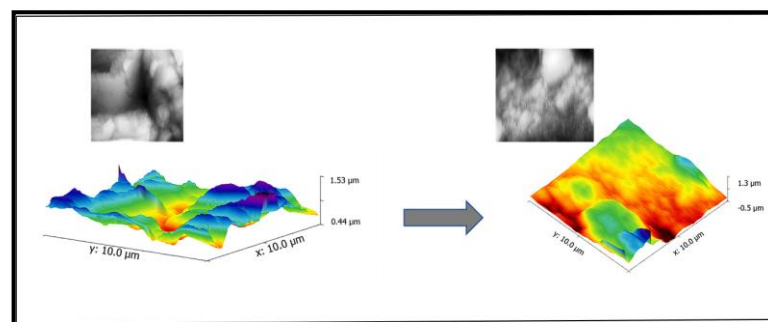


**Figure 4.** Atomic Force Microscopy (AFM) two-dimensional (2D) and three-dimensional (3D) images were obtained for naked aluminum before and after the immersion test in 3.5% synthetic seawater.

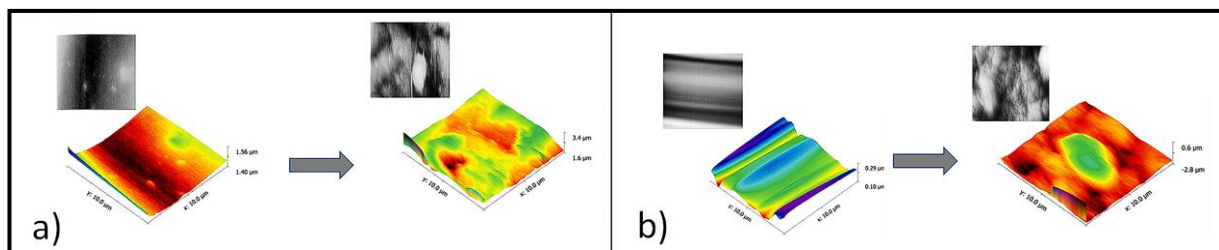


**Figure 5.** Atomic force microscopy (AFM) two-dimensional (2D) and three-dimensional (3D) images were obtained for (a) HMW-Chi and (b) HMW-Chi/PTA before and after immersion in 3.5% synthetic seawater.

The HMW-chi/PTA coating exhibited an increase in Ra from 42.65 nm to 202.02 nm before and after immersion in the corrosive medium, respectively, this can be depicted in Figure 5b. This indicates a significant increase in roughness after exposure to synthetic seawater.

On the other hand, AFM analysis of the HMW-chi/PEG coatings yields a Ra of 47.94 nm before and 332.05 nm after immersion time, as evidenced in Figure 6a. Meanwhile, the HMW-chi/PVP coating displays a Ra of 62.92 nm before and 113 nm after immersion time, as is visible in Figure 6b. These results suggest that all HMW chitosan-based coatings experienced an increase in Ra after immersion time but to a lesser extent than the obtained for the specific case of the HMW-chi/PEG coating.

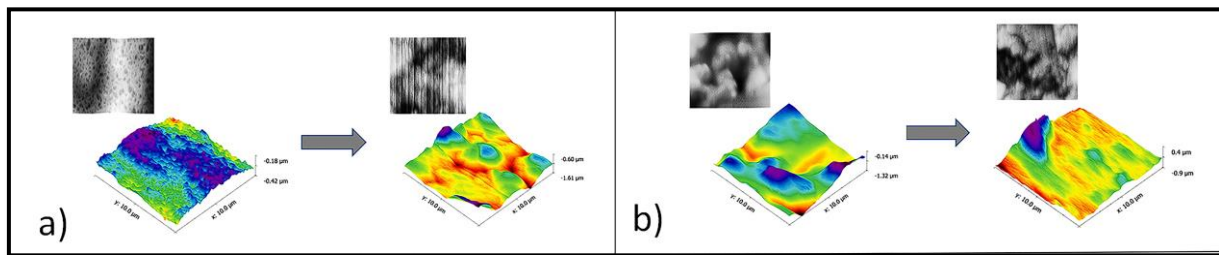


**Figure 6.** Atomic force microscopy (AFM) two-dimensional (2D) and three-dimensional (3D) images were obtained for (a) HMW-Chi/PEG and (b) HMW-Chi/PVP before and after immersion in 3.5% synthetic seawater.

Regarding the MMW-chi coatings, the MMW-chi/PTA coating exhibits a  $R_a$  of 61.37 nm and 232.21 nm before and after immersion, as illustrated in Figure 7, while the MMW-chi/PEG coating reveals a  $R_a$  roughness of 52.95 nm before and 154.75 nm after immersion time (Figure 8a). The MMW-chi/PVP coating yields a  $R_a$  of 151.21 nm before and 269.81 nm after immersion time, respectively (Figure 8b).

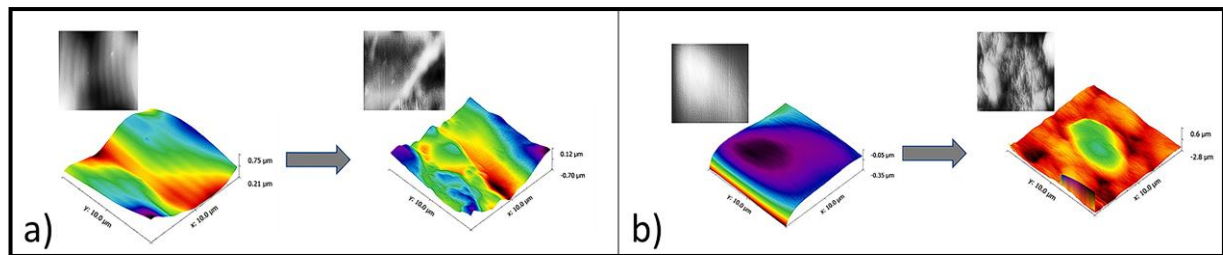


**Figure 7.** Atomic force microscopy (AFM) two-dimensional (2D) and three-dimensional (3D) images were obtained for (a) MMW-Chi and (b) MMW-Chi/PTA before and after immersion in 3.5% synthetic seawater.

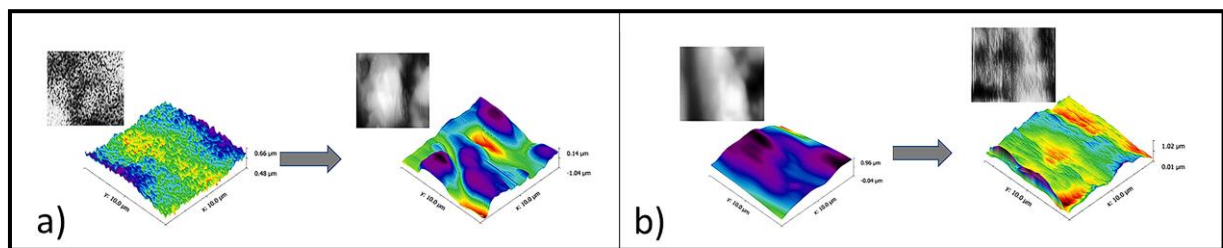


**Figure 8.** Atomic force microscopy (AFM) two-dimensional (2D) and three-dimensional (3D) images were obtained for (a) MMW-Chi/PEG and (b) MMW-Chi/PVP before and after immersion in 3.5% synthetic seawater.

It can be inferred that all coatings experienced an increase in roughness after the immersion test, which may be presumed to be related to the interaction between the coating and the aqueous medium. Roughness values were higher for medium-molecular-weight chitosan-based coatings in comparison to the higher-molecular-weight chitosan-based coatings these results are consistent with what was reported by [18].

In general, as the samples were removed from the immersion medium, their surfaces showed a noticeable increase in roughness. According to Yee et al. [60], this could be clarified by the development of irregularly shaped pits due to exposure to the saline environment for the uncoated substrates and by the chipping of the top layer of the coatings caused by exposure to aggressive conditions, resulting in changes in the surface roughness profile for the coated substrates [61].

### 3.5. Gravimetric Tests

The weight loss percentage of the coatings after immersion time in 3.5% synthetic seawater was the chosen method to evaluate the corrosion inhibition behavior according to Equation (2). The results are presented in Figures 9 and 10.

$$\text{Weight loss (\%)} = \frac{W_0 - W_1}{W_0} \times 100 \tag{2}$$

where  $W_0$  and  $W_1$  represent the weight of the samples before and after immersion, respectively.

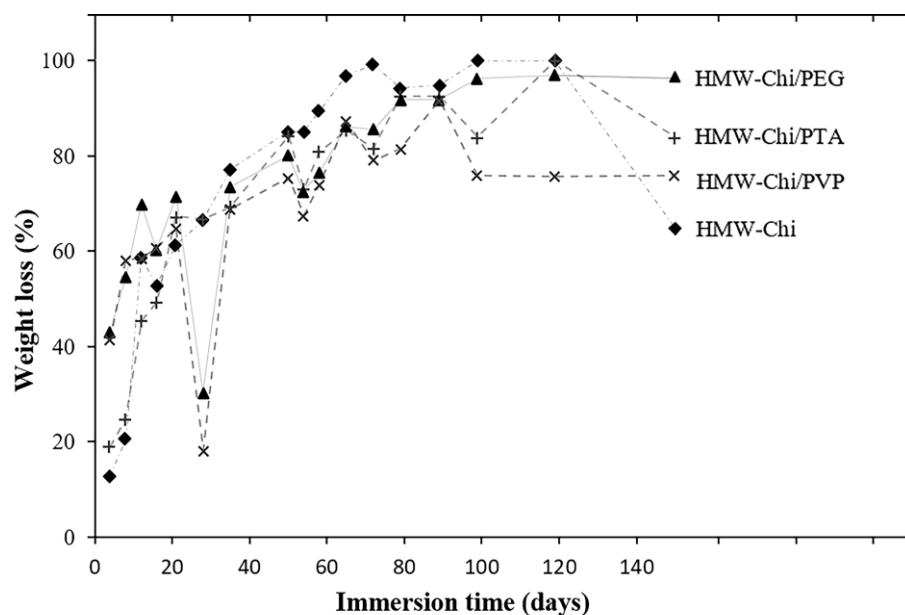


Figure 9. Weight loss percentage of high-molecular-weight chitosan-based coatings after 150 days of immersion in a solution of 3.5% synthetic seawater.

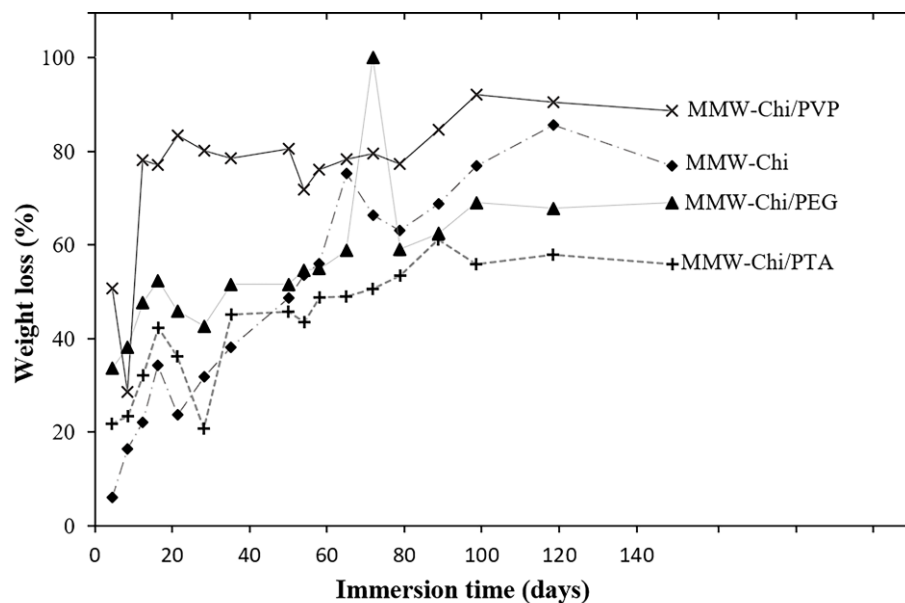


Figure 10. Weight loss percentage of medium-molecular-weight chitosan-based coatings after 150 days of immersion in a solution of 3.5% synthetic seawater.

In Figure 9, the HMW-Chi coatings exhibited a gradual increase in weight loss percentage over time. After day 21 of immersion, a decrease in the rate of weight loss was clearly observed; this may suggest that the coating reached a certain stability and provided efficient protection against corrosion. The HMW-Chi and HMW-Chi/PTA coatings yield an increase in weight loss percentage. However, the HMW-Chi/PTA coating shows a slightly lower trend in weight loss compared to HMW-Chi coatings. This could indicate that the addition of PTA to the coating improves the corrosion protection capacity of the chitosan-based coatings in terms of weight loss. HMW-Chi/PEG and HMW-Chi/PVP coatings show a gradual increase in weight loss percentage over time. However, compared to HMW-Chi and HMW-Chi/PTA, they exhibit a higher overall weight loss percentage. The above might suggest that these coatings offer lower corrosion protection.

The HMW-Chi coating exhibited a higher weight loss throughout the experiment. On the other hand, the HMW-Chi/PVP and HMW-Chi/PEG coatings displayed a minor percentage of weight loss. This may be attributed to the greater length of chitosan HMW chains that cause the polymer to expand with difficulty in the solution, hence hindering the crosslinking process [62].

Figure 10 displays the weight loss percentage behavior for the MMW based-chitosan coatings. The results for this group are comparable to those obtained for the HMW-chitosan-based coatings, highlighting a gradual increase in the weight loss percentage over time. However, the weight loss percentage seems to be lower compared to HMW-Chi coatings, indicating higher corrosion protection in terms of weight loss. Both MMW-Chi/PTA and MMW-Chi/PEG coatings showed an increase in the weight loss percentage. This occurred to a lesser extent than with the MMW-Chi coatings. This indicates an improvement in corrosion protection capacity due to the incorporation of PTA and PEG in the polymer matrix.

Unlike other MMW-Chi coatings, the MMW-Chi/PVP coating shows variability in weight loss results at different time points. This may indicate lower stability of the coating and a potential decrease in its corrosion protection capacity in terms of weight loss.

Contrary to the results obtained for the HMW chitosan-based coatings, Chi/PVP coating presented higher values of weight loss, while the MMW-Chi/PTA coating exhibited a lower percentage of weight loss, followed by the MMW-Chi/PEG coating. In general, the MMW chitosan-based coatings presented lower percentages of weight loss in contrast with the values obtained for the HMW chitosan-based coatings. As mentioned by [2], the demotion of the coating is highly related to the diffusion of salts and ions present in the medium through the coatings.

#### 4. Conclusions

High- and medium-molecular-weight chitosan and crosslinked polyethylene glycol, ammonium paratungstate, and polyvinylpyrrolidone chitosan coatings were prepared using the sol-gel technique.

The FTIR analysis confirmed the presence of functional groups and crosslinking agents in the chitosan-based coatings.

Gravimetric measurements served as a method to evaluate the corrosion inhibition behavior of chitosan-based coatings. In summary, HMW-Chi/PTA and MMW-Chi/PTA coatings appear to offer higher corrosion protection in terms of weight loss, while HMW-Chi/PEG and HMW-Chi/PVP coatings exhibit lower performance compared to the other coatings.

Overall, these findings highlight the potential of chitosan-based coatings for corrosion protection and provide valuable insights into their properties and behavior in corrosive environments.

**Author Contributions:** All authors contributed to the study's conception and design. Material preparation, data collection, and analysis were performed by A.A.A.-R., R.G.S.-D. and V.M.O.-C. The coating characterization studies before and after immersion in 3.5% synthetic seawater were carried out by Y.V.-P., G.E.D.-I. and J.Á.-S. The first draft of the manuscript was written by A.A.A.-R. and edited by R.G.S.-D. after all authors commented on previous versions of the manuscript. All authors have read and agreed to the published version of the manuscript.

**Funding:** This research was funded by project ITSON PROFAPI-2023-031 and the project CONAH-CYT Ciencia de Frontera CF-2023-G-1395.

**Institutional Review Board Statement:** Not applicable.

**Informed Consent Statement:** Not applicable.

**Data Availability Statement:** Not applicable.

**Conflicts of Interest:** The authors declare no conflict of interest.

## References

1. Verma, C.; Quraishi, M.A. Chelation capability of chitosan and chitosan derivatives: Recent developments in sustainable corrosion inhibition and metal decontamination applications. *Curr. Res. Green Sustain. Chem.* **2021**, *4*, 100184. [[CrossRef](#)]
2. Motlatle, A.M.; Mofokeng, T.G.; Scriba, M.R.; Ojijo, V.; Ray, S.S. The effect of electrically conducting carbon materials on the conductivity and morphology of poly(vinyl butyral) and chitosan blend composite for application in anti-corrosive coatings. *Synth. Met.* **2021**, *281*, 116914. [[CrossRef](#)]
3. Asadi, N.; Ramezanzadeh, M.; Bahlakeh, G.; Ramezanzadeh, B. Theoretical MD/DFT computer explorations and surface-electrochemical investigations of the zinc/iron metal cations interactions with highly active molecules from Lemon balm extract toward the steel corrosion retardation in saline solution. *J. Mol. Liq.* **2020**, *310*, 113220. [[CrossRef](#)]
4. Koch, G. Cost of corrosion. *Trends Oil Gas Corros. Res. Technol. Prod. Transm.* **2017**, *2017*, 3–30.
5. Godínez, L.A.; Meas, Y.; Ortega-Borges, R.; Corona, A. Corrosion inhibitors. *Rev. Metal.* **2003**, *39*, 140–158. [[CrossRef](#)]
6. Harb, S.V.; Trentin, A.; Uvida, M.C.; Hammer, P. Advanced organic nanocomposite coatings for effective corrosion protection. In *Corrosion Protection at the Nanoscale*; Elsevier: Amsterdam, The Netherlands, 2020; pp. 315–343.
7. Xhanari, K.; Finšgar, M. Organic corrosion inhibitors for aluminium and its alloys in acid solutions: A review. *RSC Adv. R. Soc. Chem.* **2016**, *6*, 62833–62857. [[CrossRef](#)]
8. Eduok, U.; Ohaeri, E.; Szpunar, J. Self-healing composite coatings with protective and anticorrosion potentials: Classification by healing mechanism. In *Self-Healing Composite Materials: From Design to Applications*; Elsevier: Amsterdam, The Netherlands, 2019; pp. 123–162.
9. Sambyal, P.; Ruhi, G.; Dhawan, S.K.; Bisht, B.M.S.; Gairola, S.P. Enhanced anticorrosive properties of tailored poly(aniline-anisidine)/chitosan/SiO<sub>2</sub> composite for protection of mild steel in aggressive marine conditions. *Prog. Org. Coat.* **2018**, *119*, 203–213. [[CrossRef](#)]
10. Samide, A.; Merisanu, C.; Tutunaru, B.; Iacobescu, G.E. Poly (vinyl butyral-co-vinyl alcohol-co-vinyl acetate) coating performance on copper corrosion in saline environment. *Molecules* **2020**, *25*, 439. [[CrossRef](#)]
11. Ma, Z.; Sun, M.; Li, A.; Zhu, G.; Zhang, Y. Anticorrosion behavior of polyvinyl butyral (PVB)/polymethylhydrosiloxane (PMHS)/chitosan (Ch) environment-friendly assembled coatings. *Prog. Org. Coat.* **2020**, *144*, 105662. [[CrossRef](#)]
12. Szőke, Á.F.; Szabó, G.S.; Hórvölgyi, Z.; Albert, E.; Gaina, L.; Muresan, L.M. Eco-friendly indigo carmine-loaded chitosan coatings for improved anti-corrosion protection of zinc substrates. *Carbohydr. Polym.* **2019**, *215*, 63–72. [[CrossRef](#)]
13. Bahari, H.S.; Ye, F.; Carrillo, E.A.T.; Leliopoulos, C.; Savaloni, H.; Dutta, J. Chitosan nanocomposite coatings with enhanced corrosion inhibition effects for copper. *Int. J. Biol. Macromol.* **2020**, *162*, 1566–1577. [[CrossRef](#)]
14. Sun, G.; Zhang, X.Z.; Chu, C.C. Effect of the molecular weight of polyethylene glycol (PEG) on the properties of chitosan-PEG-poly(N-isopropylacrylamide) hydrogels. *J. Mater. Sci. Mater. Med.* **2008**, *19*, 2865–2872. [[CrossRef](#)]
15. Verma, C.; Quraishi, M.A.; Alfantazi, A.; Rhee, K.Y. Corrosion inhibition potential of chitosan based Schiff bases: Design, performance and applications. *Int. J. Biol. Macromol.* **2021**, *184*, 135–143. [[CrossRef](#)]
16. Kumar, S.; Ye, F.; Dobretsov, S.; Dutta, J. Chitosan nanocomposite coatings for food, paints, and water treatment applications. *Appl. Sci.* **2019**, *9*, 2409. [[CrossRef](#)]
17. Ding, X.; Zhao, L.; Khan, I.M.; Yue, L.; Zhang, Y.; Wang, Z. Emerging chitosan grafted essential oil components: A review on synthesis, characterization, and potential application. *Carbohydr. Polym.* **2022**, *297*, 120011. [[CrossRef](#)]
18. Gouveia, Z.; Perinpanayagam, H.; Zhu, J. Development of Robust Chitosan-Silica Class II hybrid coatings with antimicrobial properties for titanium implants. *Coatings* **2020**, *10*, 534. [[CrossRef](#)]
19. Brou, Y.S.; Coulibaly, N.H.; Diki, N.G.Y.S.; Creus, J.; Trokourey, A. Chitosan biopolymer effect on copper corrosion in 3.5 wt.% NaCl solution: Electrochemical and quantum chemical studies. *Int. J. Corros. Scale Inhib.* **2020**, *9*, 182–200.
20. Ahmed, S.; Ikram, S. Chitosan & its derivatives: Are view in recent innovations. *Int. J. Pharm. Sci. Res.* **2015**, *6*, 14–30. [[CrossRef](#)]

21. Gapsari, F.; Hidayatullah, S.; Hadi Setyarini, P.; Madurani, K.A.; Hermawan, H. Effectiveness of a fish scales-derived chitosan coating for corrosion protection of carbon steel. *Egypt. J. Pet.* **2022**, *31*, 25–31. [CrossRef]
22. Ashassi-Sorkhabi, H.; Kazempour, A. Influence of fluid flow on the performance of polyethylene glycol as a green corrosion inhibitor. *J. Adhes. Sci. Technol.* **2020**, *34*, 1653–1663. [CrossRef]
23. Ramasamy, P.; Dubal, S.V.; Jeyachandran, S.; Pitchiah, S.; Kannan, K.; Elangovan, D.; Thangadurai, T.; Paramasivam, S.; Selvin, J. Control and prevention of microbially influenced corrosion using cephalopod chitosan and its derivatives: A review. *Int. J. Biol. Macromol.* **2023**, *242*, 124924. [CrossRef] [PubMed]
24. Carneiro, J.; Tedim, J.; Ferreira, M.G.S. Chitosan as a smart coating for corrosion protection of aluminum alloy 2024: A review. In *Progress in Organic Coatings*; Elsevier: Amsterdam, The Netherlands, 2015; pp. 348–356.
25. Ashassi-Sorkhabi, H.; Kazempour, A. Chitosan, its derivatives and composites with superior potentials for the corrosion protection of steel alloys: A comprehensive review. *Carbohydr. Polym.* **2020**, *237*, 116110. [CrossRef] [PubMed]
26. Sánchez-Duarte, R.G.; Sánchez-Machado, D.I.; López-Cervantes, J.; Correa-Murrieta, M.A. Adsorption of allura red dye by cross-linked chitosan from shrimp waste. *Water Sci. Technol.* **2012**, *65*, 618–623. [CrossRef]
27. Zhang, D.; Peng, F.; Liu, X. Protection of magnesium alloys: From physical barrier coating to smart self-healing coating. *J. Alloys Compd.* **2021**, *853*, 157010. [CrossRef]
28. Masuelli, M.A. Mark-Houwink Parameters for Aqueous-Soluble Polymers and Biopolymers at Various Temperatures. *J. Polym. Biopolym. Phys. Chem.* **2014**, *2*, 37–42. Available online: <https://ri.conicet.gov.ar/handle/11336/5693> (accessed on 29 May 2022).
29. Umoren, S.A.; AlAhmary, A.A.; Gasem, Z.M.; Solomon, M.M. Evaluation of chitosan and carboxymethyl cellulose as ecofriendly corrosion inhibitors for steel. *Int. J. Biol. Macromol.* **2018**, *117*, 1017–1028. [CrossRef] [PubMed]
30. Chauhan, D.S.; Mouaden, K.E.L.; Quraishi, M.A.; Bazzi, L. Aminotriazolethiol-functionalized chitosan as a macromolecule-based bioinspired corrosion inhibitor for surface protection of stainless steel in 3.5% NaCl. *Int. J. Biol. Macromol.* **2020**, *152*, 234–241. [CrossRef]
31. Chávez Huerta, A.; Rincón, M.C.; Valbuena, A.C.; López, A. Obtención y caracterización de papel de quitosano OBTENCIÓN Y CARACTERIZACIÓN DE PAPEL DE QUITOSANO. *Rev. Iberoam. Polim.* **2012**, *13*, 41–51.
32. Oliveira, J.A.M.; de Santana, R.A.C.; Neto, A.d.O.W. Characterization of the chitosan-tungsten composite coating obtained by electrophoretic deposition. *Prog. Org. Coat.* **2020**, *143*, 105631. [CrossRef]
33. Solano Romero, J.F. Obtención de Quitosano a Partir del Exoesqueleto Del Camarón (Infraorden Caridea). 2017, pp. 1–54. Available online: <http://repositorio.utmachala.edu.ec/bitstream/48000/7751/1/Mu~noz.pdf> (accessed on 22 August 2023).
34. Ubaque Beltrán, C.A.; Hernández Pedraza, S.M. *Extracción de Quitosano a Partir de Exoesqueleto de Camarón Para Elaborar Recubrimientos Para Alimentos*; SENNOVA: Bogotá, Colombia, 2018; pp. 14–51. Available online: <http://repositorio.sena.edu.co/handle/11404/5686> (accessed on 30 June 2022).
35. Colina, M.; Ayala, A.; Rincón, D.; Molina, J.; Medina, J.; Ynciarde, R.; Vargas, J.; Montilla, B. Evaluación de los procesos para la obtención química de quitina y quitosano a partir de desechos de cangrejos. Escala piloto e industrial. *Revista Iberoamericana de polímeros* **2022**, *15*, 21–43. Available online: <https://en.observatorioplastico.com/ficheros/articulos/63334929706003432.pdf> (accessed on 20 August 2023).
36. Ardean, C.; Davidescu, C.M.; Nemeş, N.S.; Negrea, A.; Ciopec, M.; Duteanu, N.; Negrea, P.; Duda-Seiman, D.; Musta, V. Factors Influencing the Antibacterial Activity of Chitosan and Chitosan Modified by Functionalization. *Int. J. Mol. Sci.* **2021**, *22*, 7449. [CrossRef] [PubMed]
37. Chen, S.; McClements, D.J.; Jian, L.; Han, Y.; Dai, L.; Mao, L.; Gao, Y. Core-Shell Biopolymer Nanoparticles for Co-Delivery of Curcumin and Piperine: Sequential Electrostatic Deposition of Hyaluronic Acid and Chitosan Shells on the Zein Core. *ACS Appl. Mater. Interfaces* **2019**, *11*, 38103–38115. [CrossRef] [PubMed]
38. Joseph, S.M.; Krishnamoorthy, S.; Paranthaman, R.; Moses, J.A.; Anandharamkrishnan, C. A review on source-specific chemistry, functionality, and applications of chitin and chitosan. *Carbohydr. Polym. Technol. Appl.* **2021**, *2*, 100036. [CrossRef]
39. Gonçalves, C.; Ferreira, N.; Lourenço, L. Production of low molecular weight chitosan and chitoooligosaccharides (COS), A review. *Polymers* **2021**, *13*, 2466. [CrossRef]
40. Villegas-Peralta, Y.; López-Cervantes, J.; Madera Santana, T.J.; Sánchez-Duarte, R.G.; Sánchez-Machado, D.I.; Martínez-Macías, M.d.R.; Correa-Murrieta, M.A. Impact of the molecular weight on the size of chitosan nanoparticles: Characterization and its solid-state application. *Polym. Bull.* **2020**, *78*, 813–832. [CrossRef]
41. Mouaden, K.E.L.; Chauhan, D.S.; Quraishi, M.A.; Bazzi, L. Thiocarbonyldiazide-crosslinked chitosan as a bioinspired corrosion inhibitor for protection of stainless steel in 3.5% NaCl. *Sustain. Chem. Pharm.* **2020**, *15*, 100213. [CrossRef]
42. Shamsheera, K.O.; Prasad, A.R.; Garvasis, J.; Basheer, S.M.; Joseph, A. Stearic acid grafted chitosan/epoxy blend surface coating for prolonged protection of mild steel in saline environment. *J. Adhes. Sci. Technol.* **2019**, *33*, 2250–2264. [CrossRef]
43. Vaz, J.M.; Taketa, T.B.; Hernandez-Montelongo, J.; Chevallier, P.; Cotta, M.A.; Mantovani, D.; Beppu, M.M. Antibacterial properties of chitosan-based coatings are affected by spacer-length and molecular weight. *Appl. Surf. Sci.* **2018**, *445*, 478–487. [CrossRef]
44. Luckachan, G.E.; Mittal, V. Anti-corrosion behavior of layer by layer coatings of cross-linked chitosan and poly(vinyl butyral) on carbon steel. *Cellulose* **2015**, *22*, 3275–3290. [CrossRef]
45. Mallakpour, S.; Jarahiyan, A. Utilization of ultrasonic irradiation as a green and effective strategy to prepare poly(N-vinyl-2-pyrrolidone)/modified nano-copper (II) oxide nanocomposites. *Ultrason. Sonochem.* **2017**, *37*, 128–135. [CrossRef]
46. Gutiérrez, T.J.; Alvarez, V.A. Nanoparticles for hyperthermia applications. *Handb. Nanomater. Ind. Appl.* **2018**, *4*, 563–576.

47. El-Aassar, M.; Ibrahim, O.M.; Fouda, M.M.; Fakhry, H.; Ajarem, J.; Maooda, S.N.; Allam, A.A.; Hafez, E.E. Wound dressing of chitosan-based-crosslinked gelatin/polyvinyl pyrrolidone embedded silver nanoparticles, for targeting multidrug resistance microbes. *Carbohydr. Polym.* **2021**, *255*, 117484. [[CrossRef](#)]
48. Mohanapriya, S.; Raj, V. Cesium-substituted mesoporous phosphotungstic acid embedded chitosan hybrid polymer membrane for direct methanol fuel cells. *Ionics* **2018**, *24*, 2729–2743. [[CrossRef](#)]
49. Kalpakli, A.O.; Arabaci, A.; Kahruman, C.; Yusufoglu, I. Thermal decomposition of ammonium paratungstate hydrate in air and inert gas atmospheres. *Int. J. Refract. Met. Hard Mater.* **2013**, *37*, 106–116. [[CrossRef](#)]
50. Pecoraro, C.M.; Santamaria, M.; Bocchetta, P.; Di Quarto, F. Influence of synthesis conditions on the performance of chitosan–Heteropolyacid complexes as membranes for low temperature H<sub>2</sub>–O<sub>2</sub> fuel cell. *Int. J. Hydrog. Energy* **2015**, *40*, 14616–14626. [[CrossRef](#)]
51. Fait, M.J.G.; Lunk, H.J.; Feist, M.; Schneider, M.; Dann, J.N.; Frisk, T.A. Thermal decomposition of ammonium paratungstate tetrahydrate under non-reducing conditions: Characterization by thermal analysis, X-ray diffraction and spectroscopic methods. *Thermochim. Acta* **2008**, *469*, 12–22. [[CrossRef](#)]
52. Peter, S.; Lyczko, N.; Gopakumar, D.; Maria, H.J.; Nzihou, A.; Thomas, S. Chitin and Chitosan Based Composites for Energy and Environmental Applications: A Review. *Waste Biomass Valoriz.* **2021**, *12*, 4777–4804. [[CrossRef](#)]
53. Dabóczy, M.; Albert, E.; Agócs, E.; Kabai-Faix, M.; Hórvölgyi, Z. Bilayered (silica–chitosan) coatings for studying dye release in aqueous media: The role of chitosan properties. *Carbohydr. Polym.* **2016**, *136*, 137–145. [[CrossRef](#)]
54. Gatto, M.; Ochi, D.; Yoshida, C.M.P.; da Silva, C.F. Study of chitosan with different degrees of acetylation as cardboard paper coating. *Carbohydr. Polym.* **2019**, *210*, 56–63. [[CrossRef](#)]
55. Gunbas, I.D.; Aydemir Sezer, U.; Gülce, I.S.; Deliloğlu Gürhan, I.; Hasirci, N. Semi-IPN Chitosan/PEG Microspheres and Films for Biomedical Applications: Characterization and Sustained Release Optimization. *Ind. Eng. Chem. Res.* **2012**, *51*, 11946–11954. [[CrossRef](#)]
56. Bakmaz, D.; Ulu, A.; Koytepe, S.; Ates, B. Preparation, characterization, and in vitro release study of vincristine sulfate-loaded chitosan–polyethylene glycol–oleic acid composites. *Int. J. Polym. Anal. Charact.* **2021**, *26*, 291–308. [[CrossRef](#)]
57. Hu, Y.; Yuan, B.; Cheng, F.; Hu, X. NaOH etching and resin pre-coating treatments for stronger adhesive bonding between CFRP and aluminium alloy. *Compos. B Eng.* **2019**, *178*, 107478. [[CrossRef](#)]
58. Zhang, Q.H.; Hou, B.S.; Li, Y.Y.; Zhu, G.Y.; Liu, H.F.; Zhang, G.A. Two novel chitosan derivatives as high efficient eco-friendly inhibitors for the corrosion of mild steel in acidic solution. *Corros. Sci.* **2020**, *164*, 108346. [[CrossRef](#)]
59. Srivastava, V.; Chauhan, D.S.; Joshi, P.G.; Maruthapandian, V.; Sorour, A.A.; Quraishi, M.A. PEG-Functionalized Chitosan: A Biological Macromolecule as a Novel Corrosion Inhibitor. *ChemistrySelect* **2018**, *3*, 1990–1998. [[CrossRef](#)]
60. Yee, Y.P.; Saud, S.N.; Hamzah, E. Pomelo Peel Extract as Corrosion Inhibitor for Steel in Simulated Seawater and Acidic Mediums. *J. Mater. Eng. Perform.* **2020**, *29*, 2202–2215. [[CrossRef](#)]
61. Kotnarowska, D.; Żabińska, A. Influence of aqueous sodium chloride solutions on operational properties of epoxy coatings. *Eksploat. Niezawodn.* **2022**, *24*, 629–640. [[CrossRef](#)]
62. Gnus, M. Influence of Chitosan molecular weight and degree of deacetylation on membrane physicochemical and separation properties in ethanol dehydration by the vapour permeation process. *Prog. Chem. Appl. Chitin Deriv.* **2020**, *25*, 79–93. [[CrossRef](#)]

**Disclaimer/Publisher’s Note:** The statements, opinions and data contained in all publications are solely those of the individual author(s) and contributor(s) and not of MDPI and/or the editor(s). MDPI and/or the editor(s) disclaim responsibility for any injury to people or property resulting from any ideas, methods, instructions or products referred to in the content.